ELSEVIER

Surface Science 498 (2002) 89–104

SURFACE SCIENCE

www.elsevier.com/locate/susc

Structure and electronic properties of CH_3- and CF_3-terminated alkanethiol monolayers on Au(1 1 1): a scanning tunneling microscopy, surface X-ray and helium scattering study

J. Pflaum [a,*], G. Bracco [b], F. Schreiber [c], R. Colorado Jr. [d], O.E. Shmakova [d], T.R. Lee [d], G. Scoles [e], A. Kahn [a]

[a] *Department of Electrical Engineering, Princeton University, Princeton, NJ 08544, USA*
[b] *Department of Physics, University of Genova and INFM, 16146 Genova, Italy*
[c] *Institut für Theoretische und Angewandte Physik, Universität Stuttgart, 70550 Stuttgart and Max-Planck-Institut für Metallforschung, 70569 Stuttgart, Germany*
[d] *Department of Chemistry, University of Houston, TX 77204-5641, USA*
[e] *Department of Chemistry, Princeton University, Princeton, NJ 08544, USA*

Received 23 March 2001; accepted for publication 31 July 2001

Abstract

The structure and the electronic properties of a series of CH_3- and CF_3-terminated alkanethiol monolayers on Au(1 1 1) have been studied by scanning tunneling microscopy (STM) and surface X-ray and helium scattering. At full coverage, the CH_3-terminated monolayers form long-range ordered domains of a $(\sqrt{3} \times \sqrt{3})R30°$ and a $(2\sqrt{3} \times 3)R30°$ standing-up phase. By thermal desorption, distinct lying-down phases of intermediate density as well as the $(p \times \sqrt{3})$ lying-down phase were generated. In contrast, the CF_3-terminated monolayers at full coverage form a standing-up phase of hexagonal symmetry that exhibits no long-range order at room temperature. Even after annealing, the domain sizes are smaller by more than one order of magnitude compared to the CH_3-terminated thiol monolayers. A comparison of the low-density lying-down phases suggests no measurable influence of the CF_3-group on the ordering. The current–voltage dependence (I–V-curves) measured by scanning tunneling spectroscopy (STS) shows no voltage gap for CH_3-terminated decanethiols. In contrast, in the I–V-curves for CF_3-terminated decanethiol monolayers, an asymmetric voltage gap of about 2 V can be clearly observed. The latter results are discussed in terms of a microscopic model that includes the formation of an interfacial Coulomb barrier at the CF_3/vacuum boundary. In addition, the effects of the tunneling conditions on the STM image contrast were examined. These studies demonstrate that the nature of the STM images and thus, the respective apparent lateral order of the films, strongly depends on the choice of the tunneling parameters.

Keywords: Self-assembly; Halogens; Surface structure, morphology, roughness, and topography; Surface electrical transport (surface conductivity, surface recombination, etc.); Scanning tunneling microscopy; X-ray scattering, diffraction, and reflection; Noble gases

* Corresponding author. Present address: Fakultät für Physik, 3 Physikalisches Institut, Universität Stuttgart, D-70569 Stuttgart, Germany. Tel.: +49-711-685-5228; fax: +49-711-685-5281.
E-mail address: pflaum@physik.uni-stuttgart.de (J. Pflaum).

0039-6028/01/$ - see front matter
PII: S0039-6028(01)01495-9

1. Introduction

The capacity for endgroup functionalization makes monolayer films formed from alkanethiols attractive candidates as linkages between an underlying substrate and, for example, molecular overlayers, proteins, and nanodots. In addition, it is well established that, on single crystalline substrates such as Au(1 1 1), alkanethiols self-assemble in large, structurally well-defined, domains [1,2]. In this context, knowledge of the structural and electronic properties of the single thiol molecules and of the complete thiol monolayer used as a template is crucial for use as building blocks (e.g., for the modification of charge injection) in microelectronic devices [3].

However, as we demonstrate in this paper, even a minor change in the chemical composition (i.e., the functional endgroup) of the thiol molecules can give rise to significant changes in the structure and the electronic properties of self-assembled monolayers (SAMs). As a consequence, engineering specific properties of thiol-based SAMs requires consideration of the interplay between the desired functionality and its possible influence on the structural features of the film. In addition to these 'engineering' considerations, a comprehensive understanding of the growth kinetics of SAMs at the microscopic level as well as of the electronic transport along the molecules is still in progress. Basic questions such as those concerning the chemisorption of the sulfur-headgroups on the Au(1 1 1) surface or the role of the chemical composition on the electron transport across the SAM are still under discussion [2,4,5].

In this paper we present a comparative study of CH_3- and CF_3-terminated alkanethiol films, examining both their ability to form well-ordered SAMs and their electronic transport characteristics. The motivation for the choice of these two endgroups was threefold. First, fluorocarbon-terminated molecular layers offer unique surface properties such as substantially lower surface energies and enhanced interfacial friction compared to their CH_3-terminated analogues [6,7]. Given that differences in hydrogen-bonding or effects due to the different polar character of the CH_3- and CF_3-terminations are unlikely causes of the differences in friction [8], the observed enhancement has been attributed to the larger van der Waals (vdW) radius of the CF_3-endgroup compared to the CH_3-termination [7,9]. As the packing densities of molecules with identical chain lengths but different terminations (i.e., CF_3 vs. CH_3) were found to be indistinguishable by atomic force microscopy (AFM), the increase of friction in the case of CF_3-terminated SAMs has been related to an increase in the interaction between adjacent CF_3-endgroups [7].

Second, the large electronegativity of fluorine and the electronic properties of its organic derivatives are likely to have a major impact on the electronic transport along the chemically modified SAMs.

Third, we wish to compare the structural and electronic parameters of these two types of SAMs to probe the origin of the contrasting "odd–even" wettability behavior exhibited by CF_3- vs. CH_3-terminated SAMs on gold, which has been attributed to the presence of strong interfacial dipoles for only the former SAMs [10,11].

Given these objectives, we have analyzed a series of SAMs on Au(1 1 1) derived from CH_3- and CF_3-terminated thiols by using three highly complementary structure-sensitive techniques: high resolution scanning tunneling microscopy (STM) and surface X-ray diffraction (GIXD) and Helium scattering.

The paper is organized in the following manner. Section 2 describes the sample preparation and characterization methods. Section 3 presents the results of the structural characterization and Section 4 describes the electronic properties of the SAMs. Finally, Section 5 discusses the collective results on the basis of a microscopic model.

2. Experimental

The thiol monolayers studied in this paper were grown on Au(1 1 1) single crystal surfaces. In order to deposit the thiols under identical conditions of substrate cleanliness and lateral coherence of the Au(1 1 1) terraces, the substrate was prepared in each case by alternating cycles of Ar^+ sputtering (0.5 keV beam energy for 10 min) and annealing

(~775 K for 30 min). The final annealing lasted for 30 min and was followed by controlled cooling to room temperature in about 30 min. Cleaning and annealing of the Au(1 1 1) surface were performed in ultra-high vacuum (UVH) at a base pressure of 5×10^{-11} Torr. The cleanliness of the gold surface and its structural ordering were confirmed following the final annealing by Auger electron spectroscopy (AES), low energy electron diffraction (LEED), and STM. The Au surface exhibited a well-defined hexagonal symmetry. Halos of triangular shape around the (1×1) main spots of the hexagonal LEED pattern indicated the formation of the $(22 \times \sqrt{3})$ reconstruction of the Au surface. The latter was also confirmed by STM. The average width of the Au surface terraces was found to be of the order of ~1500 Å. Additional in-plane diffraction peaks related to the Au reconstruction were identified by X-ray diffraction performed at the National Synchrotron Light Source (NSLS) at Brookhaven [12] and by He diffraction [13].

The thiol SAMs were grown either in solution or by vapor deposition. In the case of solution deposition, the Au crystal was transferred immediately from the UHV system into a ~1 mM solution of the CH_3- or CF_3-terminated alkanethiols dissolved in ethanol. After 24 h at room temperature, the crystal was removed from the solution, rinsed in pure ethanol, blown dry under a flow of nitrogen and transferred back to the UHV system in less than 5 min.

The thiol deposition from the gas phase was carried out in the load-lock section of the UHV system. To enable a high molecular flux at the surface of the crystal, a nozzle with a diameter less than 1 mm located 5–10 mm above the Au substrate was used. The partial pressure in the load-lock during deposition was estimated to be about 10^{-7} Torr. This value takes into account that the reading of the ion gauge in the case of decanethiol is increased by about one order of magnitude compared to the actual pressure [14].

The STM measurements were performed with a combined room temperature STM/AFM system manufactured by Omicron. The STM tips were prepared by dc-etching of tungsten wire in KOH (2 M), followed by repeated dips in HF (50% aqueous) for several seconds to remove the overlayer of tungsten-oxide. To detect effects of any remaining tungsten-oxide layer on the recorded voltage–current curves, reference measurements were performed with mechanically cut PtIr tips, which are relatively resistant to oxide formation. We found no significant differences between the two types of tips, and thus inferred the absence of an oxide layer on the tungsten tips. All STM data presented in this paper are unfiltered raw data, which have been corrected only by subtracting an averaged background for each scan line. For the derivatives of the current–voltage (I–V) spectroscopic curves, averaging over two nearest neighbor points was performed in order to suppress statistical background effects, which are appreciable especially in the small current range. In the following, the polarity of the bias voltage is referred to the sample (i.e., a positive voltage defines tunneling of electrons into the organic layer and vice versa). The spectroscopic measurements were performed with the STM feedback loop switched off.

The CH_3-terminated alkanethiols examined in this study were commercially available, and the CF_3-terminated alkanethiols were synthesized using established procedures [15].

The chain lengths of the methyl-terminated thiols ($CH_3C_{n-1}H_{2n-1}SH$) and of the fluorine-terminated thiols ($CF_3C_{n-1}H_{2n-1}SH$) range from $n =$ 10–15 and, in the following, the two compounds are referred to as CnH and CnF, respectively. As the minimum tunnel current of 10 pA, allowed by our microscope, limits the use of long chain compounds and because of the difficulties in synthesizing ω-fluorinated thiols with chain lengths shorter than 10 carbon atoms, our STM studies predominately utilized SAMs derived from the C10H and C10F adsorbates.

3. Structural properties

3.1. Standing-up phase of CnH

A representative STM image of a C10H monolayer deposited from solution is shown in Fig. 1a. To improve the lateral domain sizes of the standing-up molecules, the as-prepared films were annealed at 355 ± 5 K for several hours. On this

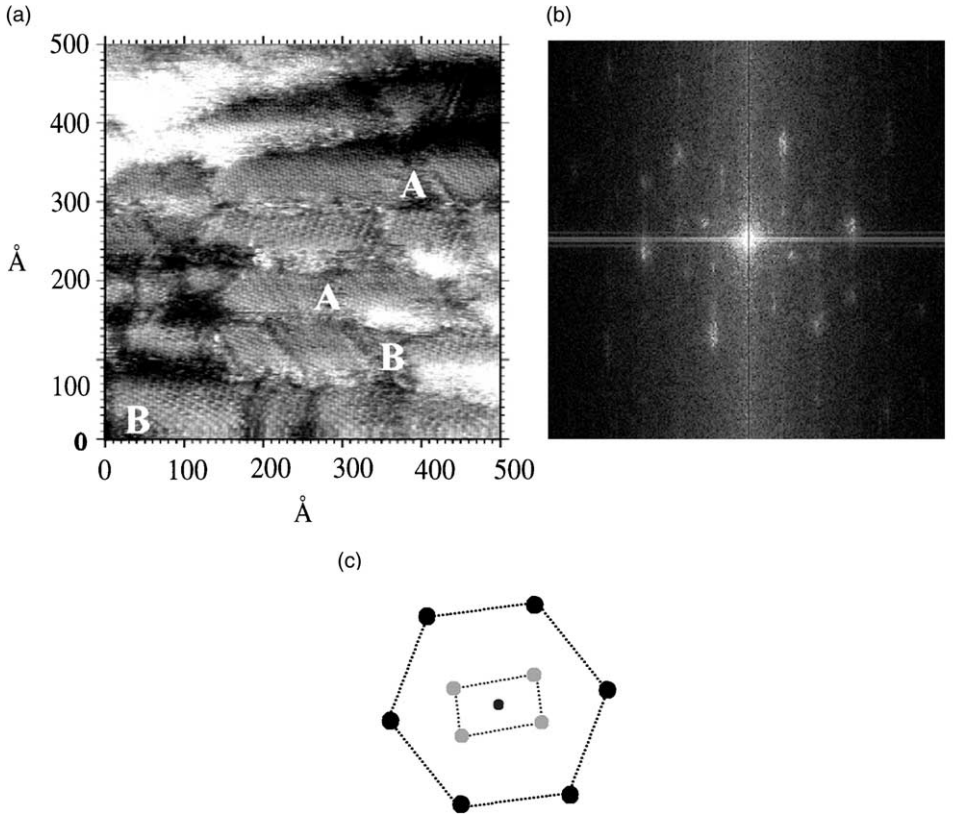

Fig. 1. (a) Standing-up phase of the C10H SAM after annealing. Areas of hexagonal $(\sqrt{3}\times\sqrt{3})R30°$ order (A) coexist with $(2\sqrt{3}\times 3)R30°$ ordered patches (B). STM data: 500×500 Å^2, $U_{gap}=-1.61$ V, $I=30$ pA. (b) Fourier transformation of (a). In the corresponding scheme (c) two sets of spots, related to the hexagonal $(\sqrt{3}\times\sqrt{3})R30°$ phase (black circles) and to the rectangular $(2\sqrt{3}\times 3)R30°$ phase (gray circles) of the C10H SAM, can be identified.

scale, the long-range lateral order of the standing-up molecules can be resolved. The linear domain sizes were found to be as large as 500 Å and, therefore, might be restricted by the width of the underlying Au terraces. Our observations indicate that the hexagonal $(\sqrt{3}\times\sqrt{3})R30°$ phase coexists with a rectangular $(2\sqrt{3}\times 3)R30°$ superstructure (for the latter, the notation $c(4\times 2)$ can also be found in literature), as previously reported [2]. In Fig. 1a, single CH_3-endgroups can be resolved in the $(\sqrt{3}\times 3)R30°$ domains (areas labeled A) and in the domains showing the $(2\sqrt{3}\times 3)R30°$ superstructure (areas labeled B). The corresponding Fourier transformation (FT) in Fig. 1b consists of spots related to both structures, as illustrated by the schematic drawing of the FT image in Fig. 1c.

To study the alignment and the ordering of the adsorbed thiols in greater detail, we performed small area scans. The topographic image of several domains with their boundaries and an observed Au vacancy island is shown in Fig. 2a. The distance between nearest neighbors in the $(\sqrt{3}\times\sqrt{3})R30°$ phase is ~5 Å, yielding an area per molecule of about 21.6 Å^2. The corresponding tilt angle of ~30° for the thiol backbones in the densely packed phase is consistent with data obtained by IR measurements [16,17].

The dark triangular spot in Fig. 2a corresponds to a single Au vacancy island. Many such islands were found to cover the surface after deposition of the thiol molecules onto the Au substrate, regardless of the chain length or nature of the alkyl terminus (i.e., CH_3 vs. CF_3). These vacancy islands

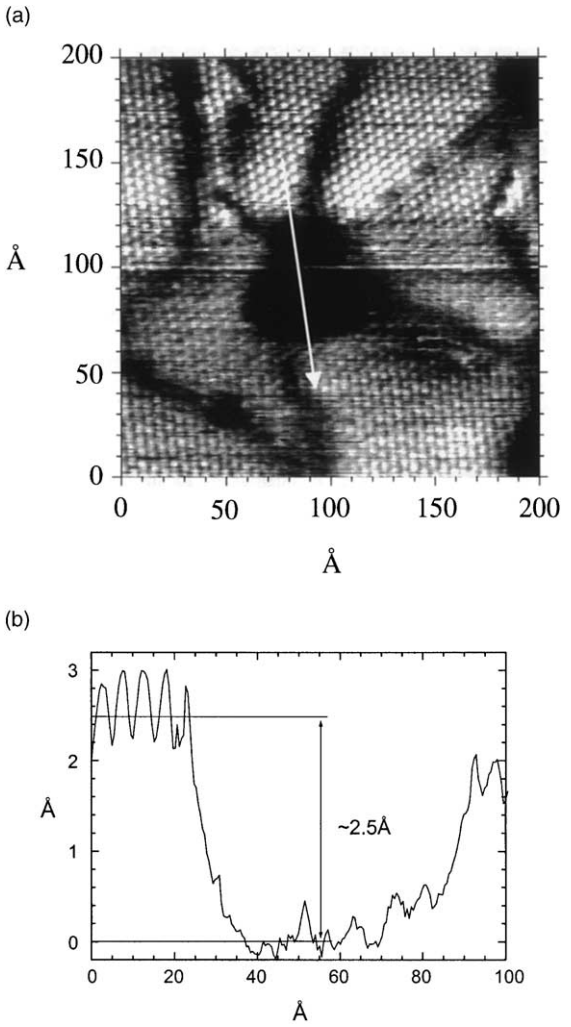

Fig. 2. (a) Single Au vacancy island surrounded by domains of $(\sqrt{3} \times \sqrt{3})R30°$ ordered C10H molecules. Molecules located in the domain boundaries show a dark STM-contrast due to a larger tilt angle compared to molecules in the domains. STM data: 200×200 Å^2, $U_{gap} = -1.76$ V, $I = 26$ pA. (b) STM line profile scanned across the pit of (a) indicating the monoatomic step depth (~2.5 Å) of the Au vacancy island.

were observed for films prepared from solution as well as from the gas phase and are related to a rearrangement of the Au surface atoms during the chemisorption of the sulfur-headgroups [18,19]. The line profile in Fig. 2b indicates that the vacancy islands are ~2.5 Å deep, in agreement with the interplane distance of 2.36 Å in the fcc Au crystal along the [1 1 1] direction. Although the distribution of the vacancy islands appears to be arbitrary, one can expect the onset of the lifting of the Au$(22 \times \sqrt{3})$ reconstruction at the bridge sites that separate the fcc–hcp–fcc structural domains, because the bonds are weaker at these positions [20]. For films grown from solution, vacancy islands deeper than a single Au atomic step were also found [21]. From the profile, we conclude that the pits are completely filled with standing-up thiol molecules.

3.2. Standing-up phase of CnF

Monolayers of C10F on Au(1 1 1) were prepared by adsorption from solution and from the gas phase. The as-prepared C10F films display standing-up C10F molecules together with Au vacancy islands having population densities and sizes comparable to the previous case. In contrast to C10H, however, no long-range order could be observed even after moderate annealing at 355 ± 5 K for several hours. A representative STM image of an annealed film is shown in Fig. 3a. Single-phase domains with dimensions of at most 50 Å can be observed, separated by boundaries and Au vacancy islands. Within the domains, the order of the molecules appears to be more perturbed and the domain edges less well-defined than for C10H.

The observed distortion of the lateral ordering can be related to the delicate balance between the relatively large vdW radius of the CF_3-endgroups ($r_{CF3} = 2.7$ Å), which is larger by ~35% compared to the case of CH_3-termination ($r_{CH3} = 2.0$ Å) [22], the spacing of the adsorption sites, and the equilibrium chain–chain distance. The steric constraints imposed by the fluorinated endgroup can plausibly lead to disorder particularly for short chain lengths, where the attractive interchain vdW interactions are diminished relative to molecules with long methylene backbones. Although the C10F domains appear to be randomly oriented, a rotational sixfold symmetry of the molecular pattern originating from the hexagonal symmetry of the underlying Au surface is still present. The observed molecular lattice spacing of ~5 Å is consistent with that of the C10H SAMs, and is further consistent with previous AFM measurements of CF_3-terminated SAMs on gold [7]. Fig. 3b shows

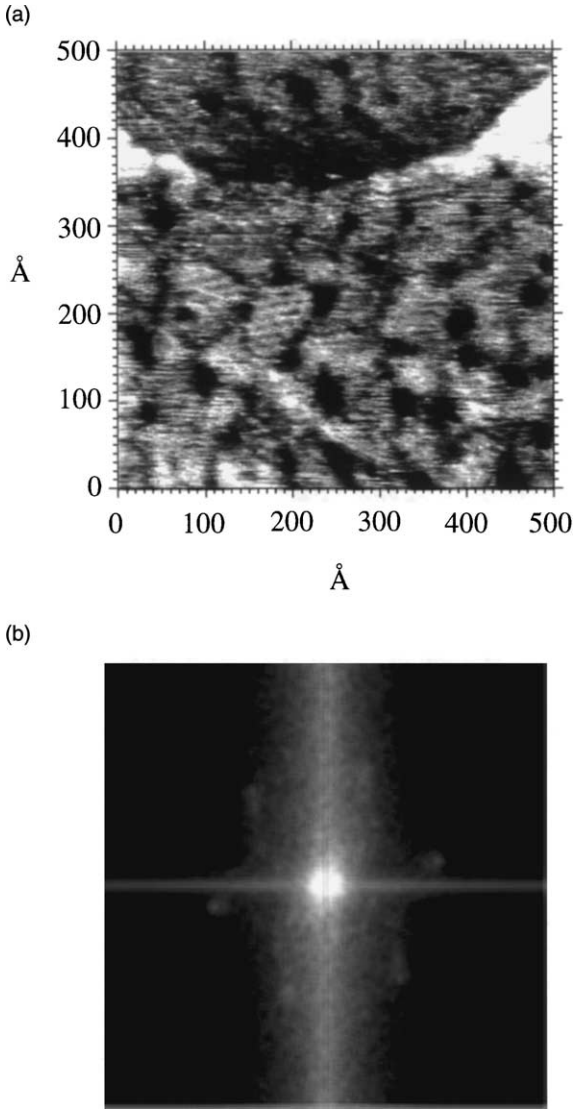

Fig. 3. (a) Monolayer of C10F after annealing. The surface consists of small partially ordered domains of molecules (diameter less than 50 Å) and several Au vacancy islands (diameters up to 30 Å). The STM scan was performed in the constant current mode (500×500 Å^2, $U_{gap} = -1.70$ V, $I = 30$ pA). (b) FT of (a). In contrast to the case of C10H (Fig. 1b), only a hexagonal pattern can be identified. The blurred spots indicate the reduced coherence of the C10F domains.

the FT of a micrograph of C10F in the standing-up configuration. The spots are considerably more diffuse than in the case of C10H (Fig. 1b) due to the inferior coherence of the lateral order.

GIXD and X-ray reflectivity measurements were carried out to gain further insight into the in-plane arrangement and the tilt angle of the molecular backbones. Extensive radial and azimuthal scans (carried out with a sensitivity sufficient to detect possible in-plane reflections with a coherence length of $\geqslant 50$ Å) led us to conclude that, for the CF_3-terminated SAMs, there is no evidence for long-range lateral ordering, neither commensurate nor incommensurate. Yet, oscillations in the reflectivity curves clearly indicate that, at full coverage, the C*n*F molecules stand upright on the Au surface. As an example, Fig. 4 shows the reflectivity curves measured for SAMs derived from C14F and C15F. By fitting the curves via Paratt formalism [23], the effective thickness, t, can be obtained and, indirectly, the tilt angle, θ, can be derived from the expected length of the molecules. The atomic distances of the geometric thiol model were assumed to be $d_{C\text{–}C} = 1.54$ Å, $d_{S\text{–}C} = 1.82$ Å, and $d_{Au\text{–}S} = 2.21$ Å, with bonding angles of $\alpha_{C\text{–}C\text{–}C} = 110°$ and $\alpha_{S\text{–}C\text{–}C} = 112°$, see Refs. [4,6,22]. The position of the SAM/vacuum interface relevant for X-ray reflectivity was set to $d_{C\text{–}F} = r_{CF3}/2 = 1.35$ Å for the CF_3-terminated SAMs, whereas for the CH_3-terminated SAMs, we assumed the position defined by the outermost carbon atom of the methylene chain.

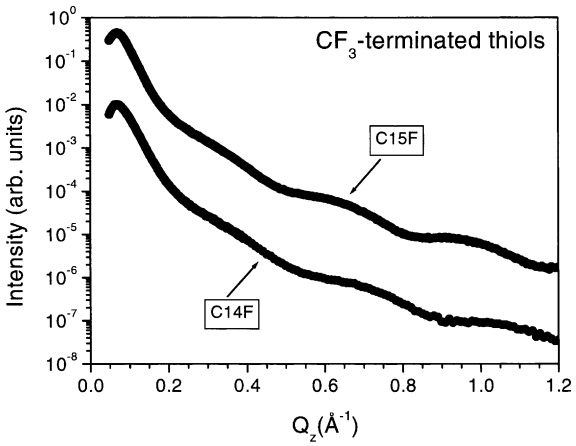

Fig. 4. X-ray reflectivity scans measured on C14F and C15F SAMs at room temperature. The scans are shifted vertically for sake of clarity. The effective thickness was estimated by fitting the oscillations of the reflectivity curves. The corresponding values are listed in Table 1.

Table 1
Comparison of the effective layer thickness, t, and the tilt angle, θ, of the CnH derived from GIXD rodscans [2,24] and of the CnF SAMs derived from the X-ray reflectivity data

n	CnH		CnF	
	t (Å)	θ (°)	t (Å)	θ (°)
10	13.2 ± 1.0	32.0 ± 0.5	13.6 ± 1.0	38.9 ± 7.0
14	17.3 ± 1.0	33.6 ± 0.35	17.9 ± 1.0	37.5 ± 4.0
15	–	–	19.3 ± 1.0	35.6 ± 4.0

The geometrical model of the alkanethiols used for the analysis is described in the text and is based on data from Refs. [4,6,22].

From structural data, we detect no influence of the preparation technique (solution vs. gas phase deposition) on either t or θ. The values for t and θ as a function of the chain length, n, are given in Table 1, along with the results for two corresponding CH_3-terminated SAMs [24]. We wish to stress, that the tilt angle and the error bars of the CnH SAMs were determined by GIXD rodscans. For a given value of n, the invariance in the values of t suggests that small systematically lower thicknesses of CF_3-terminated vs. CH_3-terminated SAMs measured by ellipsometry arise from an unidentified artifact of the latter technique [6].

The complementary data obtained by STM and GIXD show that, for the CF_3-terminated SAMs at room temperature, disorder is found not only among the functional endgroups but also within the methylene backbones. Therefore, the structural behavior of the CF_3-terminated thiol monolayers corresponds more to that of a disordered film with small coherence length rather than to a 2D crystal with long-range order as in the case of CH_3-terminated SAMs.

In addition, He diffraction on the fluorinated SAMs at full coverage indicates a commensurate well-ordered phase at 50 K. Fig. 5 shows the He-scattering intensity as a function of the in-plane momentum transfer, Q, measured for C14F-based SAMs at 50 K at different azimuthal alignments of the scattering plane between the $\langle 1\,\bar{1}\,0\rangle$ and the $\langle 1\,1\,\bar{2}\rangle$ directions of the underlying Au(1 1 1) substrate. The azimuthal width of the peaks is consistent with the out-of-plane angular resolution of the experimental setup and indicates a good crystallinity of the CF_3-terminated SAM similar to the CH_3-terminated thiol monolayers. The peaks at

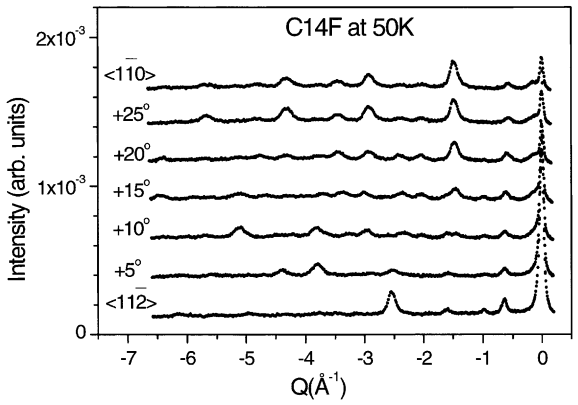

Fig. 5. In-plane diffraction pattern measured by He scattering on the C14F SAM. Within the error bar of 1.5% the diffraction peaks of the spectrum taken at 50 K can be related to the commensurate $(\sqrt{3} \times \sqrt{3})R30°$ and $(2\sqrt{3} \times 3)R30°$ phase of the SAM.

$Q = -1.47$ Å^{-1} along the $\langle 1\,\bar{1}\,0\rangle$ direction and at $Q = -2.53$ Å^{-1} along the $\langle 1\,1\,\bar{2}\rangle$ direction indicate the formation of the hexagonal $(\sqrt{3} \times \sqrt{3})R30°$ phase. Additional peaks at smaller Q-values correspond to the $(2\sqrt{3} \times 3)R30°$ superstructure. The error bar of the peak positions is on the order of 1.5%. The broadening of the specular peaks is equal to the in-plane resolution and, therefore, the average domain size is greater than the apparatus resolution width, which is about 80 Å.

The structural properties of the CF_3-terminated SAM at room temperature compared to that at 50 K suggest the existence of an order–disorder phase transition at intermediate temperatures. Unfortunately, due to the strong inelastic coupling between He and the soft chain vibrational modes, the He-diffraction intensity rapidly decreases with increasing temperature and hampers measurements in the temperature range above 50 K. Further studies by X-ray diffraction at low temperatures are in progress and will enable us to characterize the order–disorder transition in greater detail.

3.3. Lying-down phases of CnH and CnF

The influence of the functional group on the growth and the order of thiol-based SAMs in the standing-up configuration raises questions concerning the impact on the layer formation at low

coverage, where the methylene backbones tend to lie flat on the substrate. For this reason, we examined the low coverage regime for the CH_3- and CF_3-terminated thiols on gold. In both cases, the low coverages were obtained by thermally desorbing a portion of the molecules from the corresponding monolayers at full coverage. We wish to stress that partially adsorbed films might differ from partially desorbed films, and we have chosen to use the latter method of preparation, because it offers a high degree of control over the film structure [2].

The standing-up phase of a C10H monolayer annealed up to ~395 K evolves through various low-density phases to the final $(p \times \sqrt{3})$ structure, with $p = 11$. As an example, Fig. 6a shows the intermediate phase, labeled $h(5\sqrt{3} \times \sqrt{3})R30°$ [25]. The bright spots correspond to the sulfur headgroups. Because of their lower electron density as compared to the headgroups, the tails produce a rather dark contrast in the STM images. The height profile in Fig. 6b shows that the distance between each pair of rows is 22 Å, indicating some overlap of the tails of adjacent rows as proposed in Ref. [25].

The $(11 \times \sqrt{3})$ phase, a representative image of which is shown in Fig. 7a, occurs at densities less than 27% of full thiol coverage. The layer consists of stripes of thiols with two alternating sulfur-groups and two tails facing each other. From the analysis of the corresponding line profiles in Fig. 7b, the distance between the individual rows can be estimated to be about 32 Å, which agrees well with the value determined by atom diffraction [26]. In this phase, the thiol molecules are lying flat in an *all-trans* configuration on the Au(1 1 1) surface.

With respect to possible applications as organic templates in heterostructures, the question of the maximum domain size for the decanethiol lying-down phase is of great interest. In our STM measurements, the size of the largest single striped domains is restricted only by the dimensions of the Au terraces and, therefore, can exceed 1500 Å.

The thermal treatment described above was also applied to the CF_3-terminated decanethiols, and the dependence of the intermediate structural phases on the annealing procedure was indistinguishable from that observed for C10H. For example, Fig. 8a shows the $h(5\sqrt{3} \times \sqrt{3})R30°$ phase

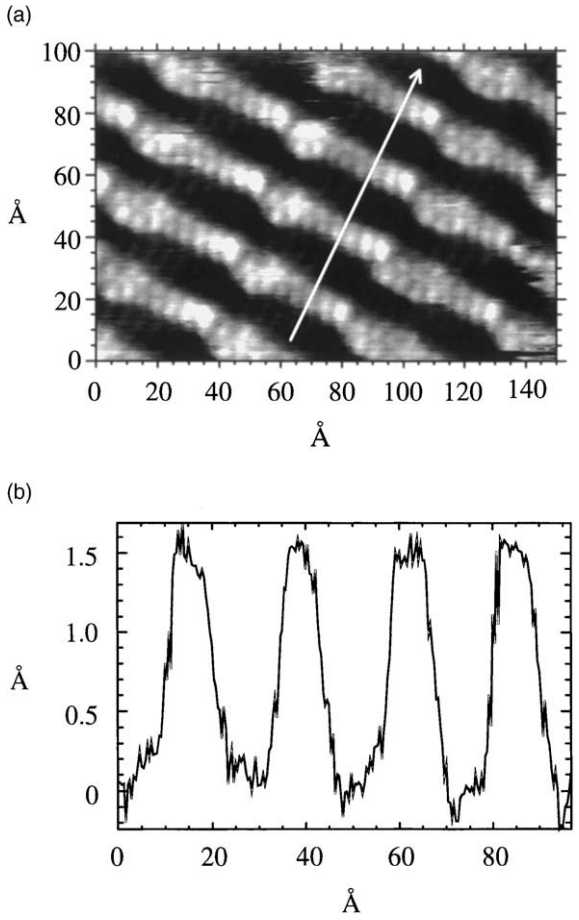

Fig. 6. (a) STM constant current mode image (150×100 Å^2, $U_{gap} = -1.70$ V, $I = 28$ pA) of an intermediate low-density phase of C10H. Following Ref. [25] this phase is labeled as $h(5\sqrt{3} \times \sqrt{3})R30°$. Due to their higher charge density, the sulfur headgroups appear as bright spherical spots, whereas the tails exhibit a darker image contrast. (b) Line profile along the molecular rows indicated by the arrow in (a). From the stripe distance of ~22 Å the conclusion can be drawn that the methylene backbones are not lying flat on the Au(1 1 1) surface.

for C10F together with a corresponding line profile in Fig. 8b. The fact that the same phases can be stabilized by thermal desorption at similar annealing temperatures for C10H and for C10F suggests a weak influence of the fluorinated end-groups on the alignment of the lying-down thiols and, therefore, on the low-density regime of the phase diagram for C10F. The assumption of a negligible constraint by the larger vdW radius of the CF_3-termination on the structural coherence in

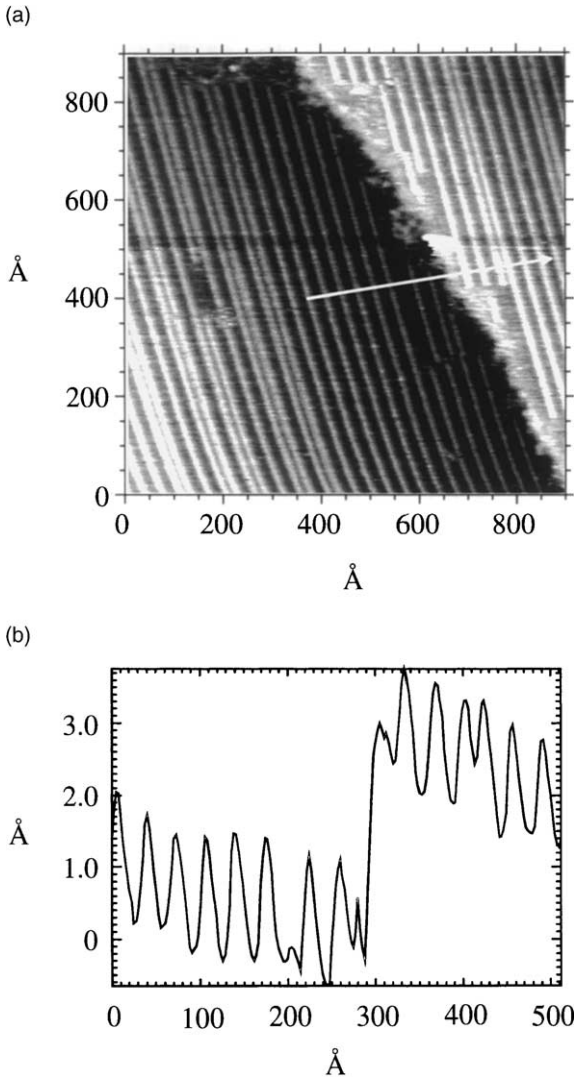

Fig. 7. (a) STM image of the low-density $p(11 \times \sqrt{3})$ striped phase (900×900 Å^2) of the C10H thiol monolayer. Scanning parameters: $U_{gap} = -1.42$ V, $I = 33$ pA. The two striped domains in this image are formed on different Au terraces separated by a monoatomic step (see (b)). The topological defect on the left side of the image results from a 180°-flip of adjacent rows. (b) Line profile along the arrow in (a). The stripe separation of 32 Å indicates a complete stretching of the thiol molecules on the Au surface in an *all-trans* configuration. The height difference of 2.5 Å in the center of the profile corresponds to the monoatomic step height between the two Au-terraces in (a).

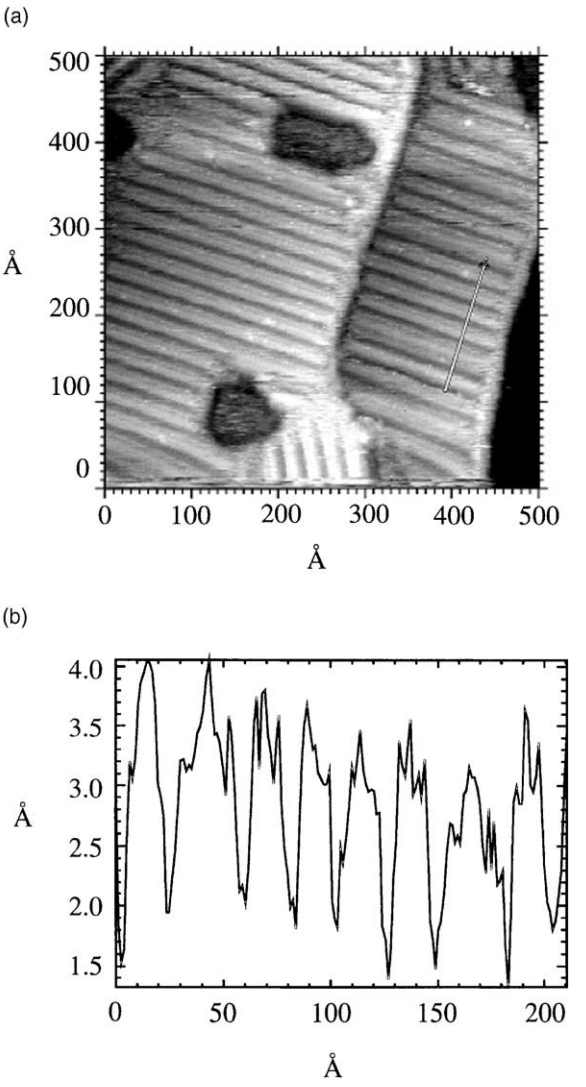

Fig. 8. (a) Intermediate low-density phase for C10F (500×500 Å^2, $U_{gap} = -1.93$ V, $I = 16$ pA). The stripe spacing of the observed pattern corresponds to the $h(5\sqrt{3} \times \sqrt{3})R30°$ structural phase [25]. Some Au vacancy islands are still present even after annealing the layers up to 395 K. (b) Line profile along the arrow in (a). Although the line spacing corresponds to the $h(5\sqrt{3} \times \sqrt{3})R30°$ phase, the profile differs slightly from the one of the C10H SAM (see Fig. 6b) due to different tunneling parameters and charge densities at the CH_3- and CF_3-end-groups.

the low coverage regime is also supported by the observation of comparable sizes of domains for both compounds. As shown in Fig. 9a, further thermal desorption of molecules leads also to an $(11 \times \sqrt{3})$ striped phase for C10F. The separation of 32 Å between the rows of sulfur heads, which is

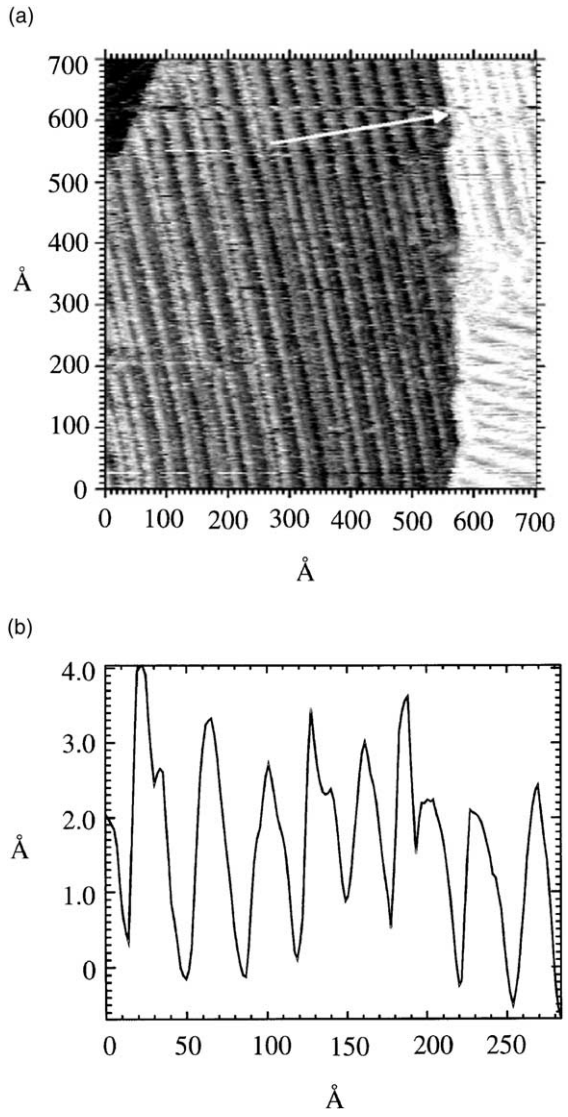

Fig. 9. (a) STM constant current scan of the $p(11 \times \sqrt{3})$ low-density phase for the C10F film (700×700 Å^2, $U_{gap} = -1.42$ V, $I = 21$ pA). (b) Line profile corresponding to the arrow in (a). The line spacing of 32 Å corresponds to the formation of the low-density lying-down phase $p(11 \times \sqrt{3})$ for C10F.

shown in Fig. 9b, agrees with the structural data obtained for C10H.

4. Electronic properties

Although it has been shown by theoretical calculations of the molecular electronic states that alkanethiols on gold act rather as insulators due to their transport gap of the order of 10 eV, as polarizable matter, they strongly influence the tunneling barrier between the substrate and the tip [27]. Initial evidence of this phenomenon was the observation of a measurable tunneling current even at tip–substrate separations of about ~18 Å, corresponding to the standing-up phase of C12H on gold at a tilt angle of ~30° [5]. In vacuum the tunneling current at this distance would be completely negligible. Second, the image contrast is sensitive to changes of the tunneling conditions. As an example, Fig. 10a and b shows the same (40×40) Å^2 area covered by the rectangular $(2\sqrt{3} \times 3)R30°$ structure of C10H imaged at slightly different gap voltages. In the constant tunnel current mode for a gap voltage of $U_{gap} = -1.40$ V, the so-called "pin-wheel" structure can be observed for which bright spots form groups of diamond-shaped facets separated by single rows of dark spots. Upon increasing the negative bias voltage to about -1.70 V, the contrast of the STM image is determined by alternating rows of dark and bright spots forming a "zig-zag" pattern on the surface. This behavior is completely reversible. Even if the microscopic origin of the image contrast is not yet clear and could be related to different electronic properties at non-equivalent adsorption sites of the sulfur, Fig. 10a and b unambiguously show that the two different $(2\sqrt{3} \times 3)R30°$ superstructures ("pin-wheel" and "zig-zag") reported in previous STM studies [28] are related to electronic effects rather than to structural differences. This interpretation is consistent with structural data obtained by X-ray diffraction in which only one superlattice at full coverage was observed [2].

For a more detailed analysis of the electron transport along the thiol molecules, we performed measurements of the I–V-curves of both CH_3- and CF_3-terminated SAMs on Au(1 1 1). During the tunneling spectroscopy, the STM feedback control was switched off. In this context, we focus here on the standing-up phases for C10H and C10F. Before we discuss the data, we note that in the case of the lying-down phases, we observed that ramping the voltage at a fixed sample tip distance led to instabilities in the tunneling conditions, resulting

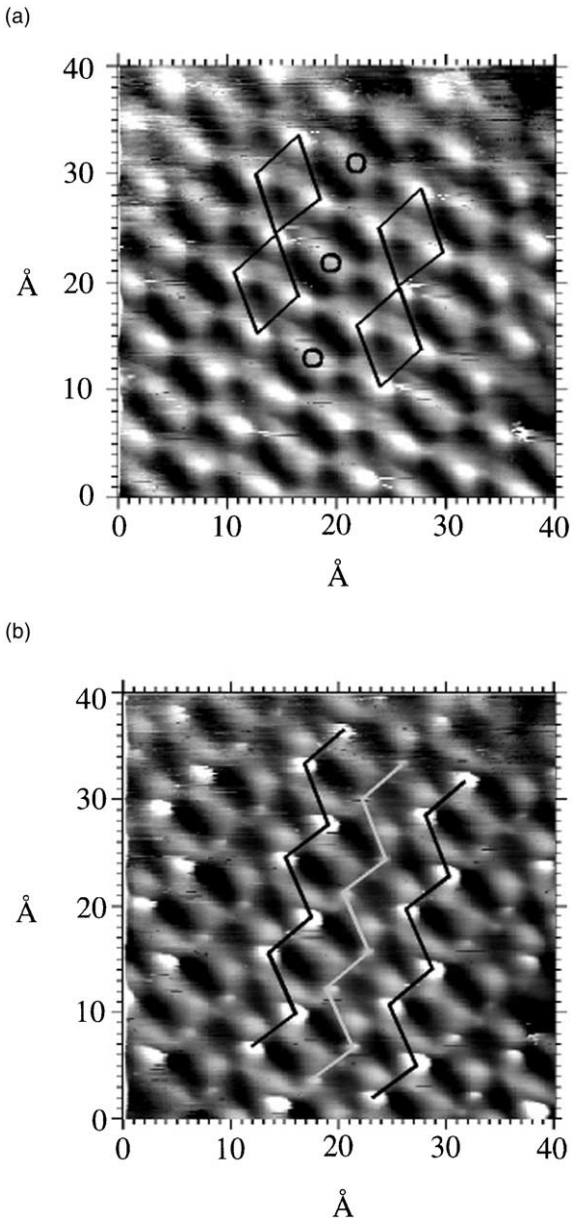

Fig. 10. (a) The "pin-wheel" structure of the $(2\sqrt{3}\times 3)R30°$ standing-up phase for the C10H SAM (STM parameters: 40×40 Å^2, $U_{gap}=-1.40$ V, $I=29$ pA). Bright spots that form diamond-like facets are separated by straight rows of spheres of darker contrast. (b) The "zig-zag" pattern of the $(2\sqrt{3}\times 3)R30°$ standing-up phase for the C10H film (STM parameters: 40×40 Å^2, $U_{gap}=-1.70$ V, $I=29$ pA). "Zig-zag" rows of bright spots alternate with rows of darker spots. The scanned areas in (a) and (b) are identical.

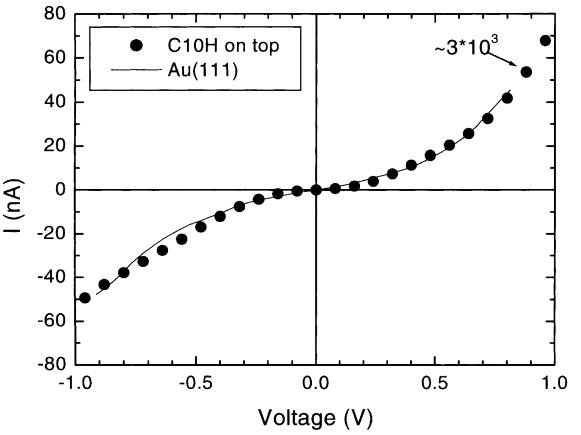

Fig. 11. I–V-curves for the bare Au(1 1 1) surface and for the C10H SAM at full coverage measured on top of the endgroups. The tunneling current data for the SAM are multiplied by a factor of 3×10^3.

in poorly reproducible I–V-data. This behavior might be due to the weak physisorption of the hydrocarbon chains to the Au surface and, therefore, to the possibility of significant tip–molecule interactions during changes of the gap voltage.

Fig. 11 shows the I–V-curves measured for the bare Au(1 1 1) surface and for the same surface covered with C10H in the standing-up configuration. The I–V-curve for C10H was taken on top of the endgroup and scaled by a proportionality factor of $\sim 3\times 10^3$. These two I–V-curves are in excellent agreement with each other. This observation supports the conclusion that the alkanethiol layer acts as a dielectric between the substrate and the tip without significant intrinsic contributions by either the endgroup or the backbone to the transport process. As a consequence of the headgroup–substrate bonding, the electronic interface conditions might also affect the transport behavior, e.g., by the possibility of charge-transfer. But for sake of simplicity, we will omit this more complex influence on the tunneling from the following discussion.

To gain more insight into the electronic transport along the molecule, we analyzed the derivative of the tunneling current with respect to the applied voltage, i.e. $\mathrm{d}I/\mathrm{d}V(V)$. The derivative, $\mathrm{d}I/\mathrm{d}V(V)$, is more sensitive to changes than $I(V)$-curves, and the peaks in the $\mathrm{d}I/\mathrm{d}V$ behavior

correspond to positions of the energy levels in the local density of states (LDOS) participating in the tunneling process. For a quantitative study of the LDOS, one would need to plot the derivative dI/dV normalized to the conductance, i.e., $(dI/dV)/(I/V)$, which is directly proportional to the LDOS [29]. But in view of the small tunneling currents used in our experiments, this quantity would strongly fluctuate, especially around $U_{gap} = 0$ V, and would possibly obscure real peaks.

Fig. 12a shows an example of a topographic image of a C10H sample area on which the I–V-behavior was measured. Due to the small scan range and the stable conditions during the spectroscopic measurements, the spatial resolution is sufficient to distinguish between the different locations at which the I–V-curves were recorded. Fig. 12b includes two $dI/dV(V)$-curves, one representative for measurements taken on top of the CH_3-endgroups (“tops”, corresponding to bright areas in Fig. 12a), and the other representative for measurements taken in the gaps between the endgroups (“holes”, corresponding to dark areas in Fig. 12a). Tunneling of electrons out of the thiol SAM (i.e., at $U_{gap} < 0$ V) shows no difference in the current–voltage dependence of the “tops” and the “holes”. Even up to $U_{gap} \approx 0.5$ V, the current characteristics for both locations are approximately the same, each showing two peaks at around -0.5 and $+0.5$ V. By comparing the measured I–V-curves with those corresponding to the bare Au substrate, the two peaks can be related to the electronic surface states of the Au(1 1 1) substrate [30]. The fact that no additional peaks appear in the dI/dV-curves suggests that no molecular states participate in the tunneling process out of the organic layer.

However, for positive voltages above 0.5 V, the dI/dV-curves for the “tops” and the “holes” exhibit pronounced differences. From the I–V-curves at $U_{gap} = 1.4 \pm 0.2$ V, the tunneling current into the endgroup of the C10H monolayer is larger by about 55% as compared to the tunneling current into the “holes”. A possible rationalization for this phenomenon can be found if the tip–molecule interaction is taken into consideration. The electrostatic interaction is expected to be more attractive for tunneling into the layer (negative tip–positive endgroup) than for tunneling out of the layer (positive tip–positive endgroup) and to be stronger on top of the molecular endgroups than in be-

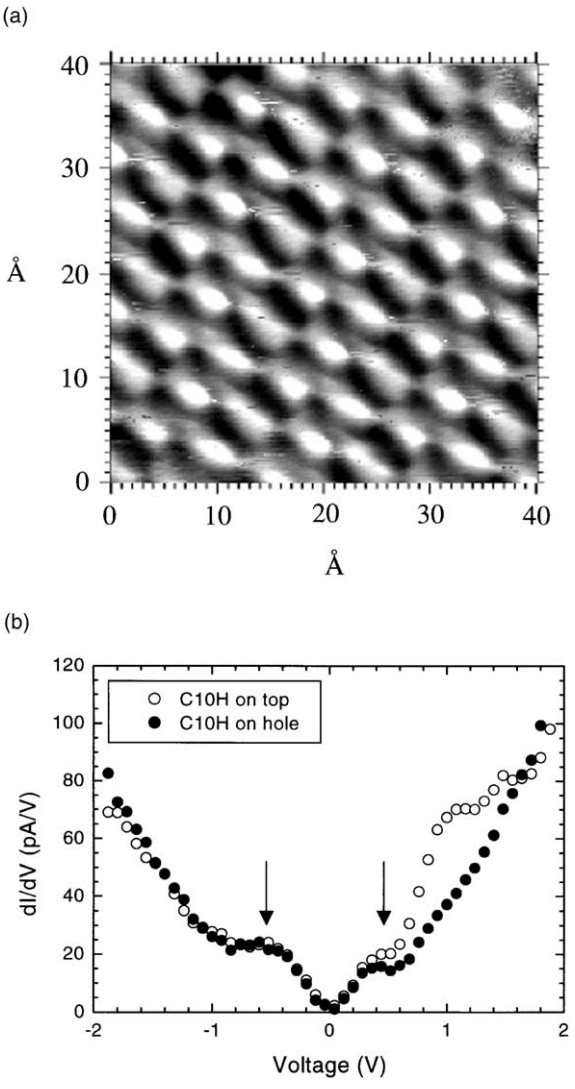

Fig. 12. (a) Topographic image of the area covered with the C10H standing-up phase on which the I–V-data were collected (STM parameters: 40×40 Å^2, $U_{gap} = -1.39$ V, $I = 29$ pA). The resolution is sufficient to distinguish the position of the endgroups (“tops”) and in between (“holes”). (b) $dI/dV(V)$-curves measured on top and in between the endgroups of the C10H standing-up phase shown in (a). Peaks related to the surface states of the underlying Au(1 1 1) surface are marked by arrows. The setpoint parameters during the I–V-measurements are given in (a).

tween. The latter results from the electron density profile at the SAM/vacuum interface. As a consequence, the attractive interaction may reduce the vacuum gap distance slightly, and, thereby increase the tunneling current. The fact that the C10H SAMs show a gapless I–V-behavior is consistent with our assumed model that alkanethiol SAMs behave as dielectric materials without intrinsic electronic contributions to the tunneling process.

The situation changes drastically by substituting the CH_3-endgroup with a CF_3-endgroup. By focusing on small, relatively ordered patches of the C10F SAMs (Fig. 13a), sufficient spatial stability was obtained to perform spectroscopic measurements. As the topographic image of the C10F SAM (Fig. 13a) is much more distorted than that of the C10H monolayer (Fig. 12a), the current–voltage characteristics were analyzed only on top of the endgroups which could be readily distinguished from the hollow sites. A representative $\mathrm{d}I/\mathrm{d}V(V)$-curve measured for the C10F SAM is shown in Fig. 13b. For the purpose of comparison, Fig. 13b also shows the $\mathrm{d}I/\mathrm{d}V(V)$ data measured on top of the endgroups of a C10H monolayer.

Two fundamental differences in the electronic properties of the two types of SAMs can be clearly distinguished. First, whereas no voltage gap can be detected for the C10H-based SAM, the $\mathrm{d}I/\mathrm{d}V(V)$-curve for the C10F SAM exhibits a plateau with a total width of 2.0 ± 0.2 V. It is important to stress that this gap is also apparent in the I–V-curves and, therefore, corresponds to a situation where $I = 0$, rather than to a constant but non-vanishing current.

Second, the voltage gap observed for the C10F SAM exhibits an asymmetry. As can be seen from Fig. 13b, the gap is shifted by $\sim$0.4 V toward positive sample voltages (i.e., tunneling into the C10F SAM is suppressed more strongly than tunneling out of it). Additionally, the two peaks in the $\mathrm{d}I/\mathrm{d}V(V)$-curves for the C10H monolayer, which had been related to the Au(1 1 1) surface states [30], cannot be detected in the case of the C10F SAM. At higher positive and negative bias voltages, the $\mathrm{d}I/\mathrm{d}V$-curve of the CF_3-terminated decanethiols shows a much steeper increase in the regime where tunneling occurs when compared to

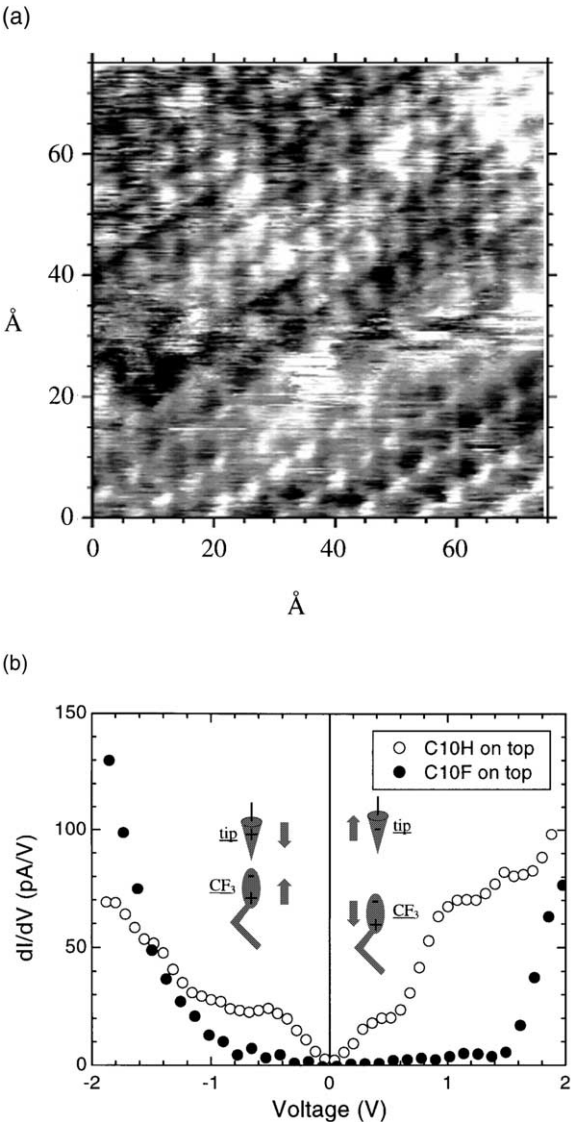

Fig. 13. (a) Constant current STM image of the standing-up phase for the C10F (75×75 Å^2, $U_{gap} = -1.87$ V, $I = 33$ pA). The image shows the area on which the I–V-data were collected. (b) Comparison between the $\mathrm{d}I/\mathrm{d}V(V)$-curves for the C10F and C10H SAMs measured on top of the respective endgroups. The curves were recorded at the same tunneling setpoints as the area scans shown in Figs. 12 and 13a.

the corresponding curve for the C10H-derived SAM. As we will discuss in the following section, the higher negative charge density at the CF_3/vacuum interface as compared to the CH_3/vacuum

interface can be attributed to the observed voltage gap and its asymmetry.

5. Discussion

As demonstrated in Sections 3 and 4, replacement of the terminal CH_3-group with a CF_3-group in alkanethiol-based SAMs on Au(1 1 1) is sufficient to generate relatively small structural changes but substantial modifications in the electronic transport properties of the SAMs. To understand these changes, we focus on the differences between the CF_3 and CH_3 endgroups, given that the sulfur headgroups and the hydrocarbon backbones remain unchanged in both SAM systems.

The substitution of hydrogen with fluorine is accompanied by an important change in the electronic structure of the endgroup. The strong electronegativity of fluorine shifts the negative charge distribution of the CF_3 endgroup toward the fluorine atoms. In contrast, the electrons are preferentially located next to the central carbon atom for the CH_3 endgroup. As a consequence, the electron density in C*n*H SAMs is concentrated along the central C–C σ-bonds of the methylene backbone, whereas the electron density in C*n*F SAMs extends toward the CF_3/vacuum interface.

To illustrate this effect, we plot in Fig. 14 the static charge distribution for decanethiols with CH_3- and CF_3-termination (calculations by HYPERCHEM 6.0 using PM3 parametrization). We stress that the calculations are intended only to give qualitative insight regarding the endgroup properties and thus make no claim for quantitative correctness. The iso-charge contourlines around the endgroup are noticeably more extended for the fluorine-terminated decanethiol than for the hydrogen-terminated decanethiol. The charge distribution at the CF_3-endgroup also suggests that, within a closed packed (hexagonal) arrangement of C10F molecules, a repulsive interaction between the CF_3-endgroups will at least partially counteract the attractive vdW interactions among the methylene chains.

As a rough approximation, we find that the radius of the charge distribution in the case of the CF_3-group is ~20% larger than that of the CH_3-group. This trend agrees qualitatively with the larger vdW radius for CF_3 ($r_{CF3} = 2.7$ Å) com-

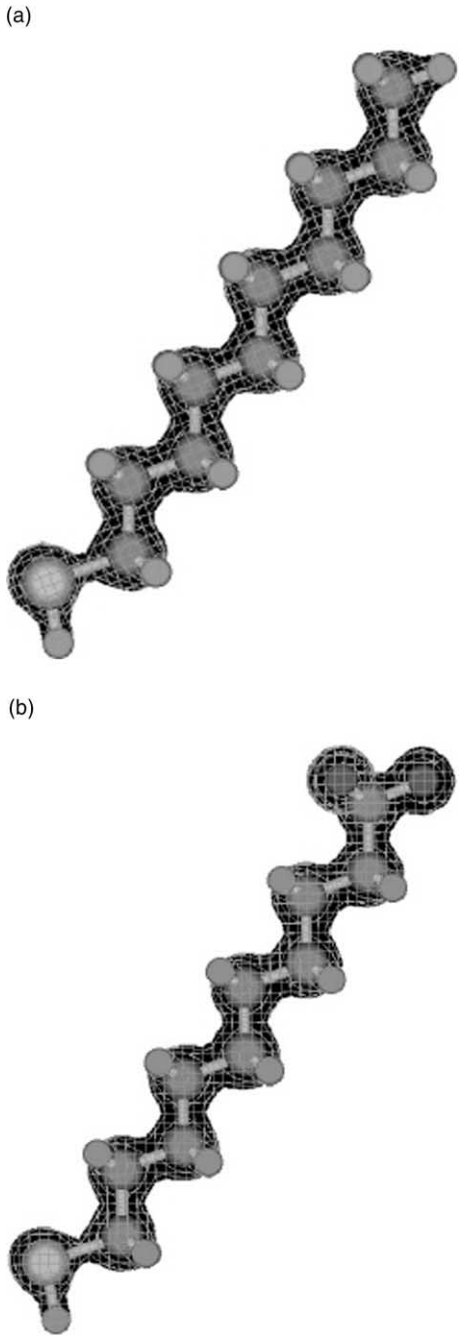

Fig. 14. Structural model showing qualitatively the charge distribution for (a) C10H and (b) C10F.

pared to CH_3 ($r_{CH3} = 2.0$ Å) [22]. Therefore, it seems plausible that the additional 'steric strain' imposed by the CF_3-group can relax by increasing the density of defects and domain boundaries of CF_3-terminated SAMs, which would be consistent with the experimentally observed smaller domain sizes for C10F SAMs vs. C10H SAMs (Figs. 3a and 1a).

In this context, we refer to Ref. [31] in which time-of-flight scattering and recoiling spectrometry (TOF–SARS) showed that an azimuthal sixfold symmetry related to the lateral ordering for C16F and C17F can be observed. Due to odd–even effects, the symmetry is much less pronounced for the C17F SAMs than for the C16F SAMs. Although, these results seem, at first glance, to contradict the data in the present paper, several aspects must be considered before comparing both studies.

First, the azimuthal asymmetry for the scattering signal for the C16F and C17F SAMs, which is determined more by the local symmetry of the lattice than by the long-range order of the SAMs [31], is small (at most on the order of ~10% of the total scattered intensity). Also, the fact that the minima and maxima in the azimuthal dependence of the signal are broadened by more than 10° is consistent with our observation of missing long-range order for the CF_3-terminated SAMs. Finally, for the C16F and C17F SAMs, we would expect less severe constraints imposed by the CF_3-endgroup since the chains are longer than that of the C10F SAM.

Our studies have also found that the CF_3-endgroup gives rise to unique transport properties (i.e., the observed voltage gap and its asymmetry; see Fig. 13b). For electrons tunneling in either direction, the enhanced electron density at the CF_3/vacuum acts as a charge barrier. Therefore, tunneling in the regime up to ±1 V is strongly suppressed and cannot be detected in the STS measurements. It is important to stress that the term "gap" in this context should not be confused with its classical definition as a state-free window of energy in the LDOS of a periodic atomic or molecular lattice. Moreover, from theoretical studies it is not expected that electronic states located along the thiol backbone or, at least at the functional CH_3-endgroup, would contribute to the tunneling current [27].

The observed asymmetry of the voltage gap must be related to a different effect, as the Coulomb barrier itself is symmetric for electrons tunneling out of the tip or out of the Au–S interface. Keeping in mind that the STM feedback control was switched off during the spectroscopic measurements, we attribute the observed asymmetry to tip–endgroup interactions. Because of the dipole formation at the CF_3/vacuum interface with the negative pole pointed toward the vacuum (see inset in Fig. 13b), we expect a much stronger interaction between the tip and the CF_3-terminated SAM surface than for the CH_3-terminated SAM surface. As a consequence, at negative bias voltages (positive tip voltages), the attractive force between the tip and the CF_3-groups causes a reduction of the vacuum gap and, therefore, supports tunneling out of the layer. On the other hand, at positive gap voltages (negative tip voltages), repulsive forces between the tip and the CF_3-groups can suppress the tunneling by slightly increasing the vacuum gap.

In conclusion, we propose that the asymmetry observed in the voltage gap for the CF_3-terminated decanethiols arises from strong tip–endgroup interactions, taking also into consideration that already small changes of the tilting of the thiols vary the tip–molecule distance sufficiently to cause big changes in the tunneling current.

Acknowledgements

The authors wish to thank A. Selloni for helpful discussions on the electronic transport behavior. The work at Princeton was supported by the MRSEC program of the National Science Foundation (DMR-9809483) and the Deutsche Forschungsgemeinschaft (Grant PF385-11 to J. Pflaum). G. Bracco acknowledges the INFM unit of Genova for support and F. Schreiber wishes to thank H. Dosch for generous support. The National Science Foundation (DMR-9700662) provided support for the research at the University of Houston. The surface X-ray studies were carried out at the National Synchrotron Light Source at the Brookhaven National Laboratory.

References

[1] A. Ulman, Introduction to Ultrathin Organic Films from Langmuir-Blodgett to Self-Assembly, Academic Press, San Diego, 1991.
[2] F. Schreiber, Prog. Surf. Sci. 65 (2000) 151.
[3] I.H. Campell, J.D. Kress, R.L. Martin, D.L. Smith, N.N. Barashkov, J.P. Ferraris, Appl. Phys. Lett. 71 (1997) 3528.
[4] P. Fenter, F. Schreiber, G. Scoles, P. Eisenberger, M.J. Bedzyk, Surf. Sci. 412/413 (1998) 213; 425 (1998) 138.
[5] L.A. Bumm, J.J. Arnold, L.F. Charles, T.D. Dunbar, D.L. Allara, P.S. Weiss, J. Am. Chem. Soc. 121 (1999) 8017.
[6] Y.F. Miura, M. Takenaga, T. Koini, M. Graupe, N. Garg, R.L. Graham Jr., T.R. Lee, Langmuir 14 (1998) 5821.
[7] H.I. Kim, M. Graupe, O. Oloba, T. Koini, S. Imaduddin, T.R. Lee, S.S. Perry, Langmuir 15 (1999) 3179.
[8] N.A. Burnhan, D.D. Dominguez, R.L. Monery, R.J. Colton, Phys. Rev. Lett. 64 (1990) 1931.
[9] H.I. Kim, T. Koini, T.R. Lee, S.S. Perry, Langmuir 13 (1997) 7192.
[10] M. Graupe, M. Takenaga, T. Koini, R. Colorado Jr., T.R. Lee, J. Am. Chem. Soc. 121 (1999) 3222.
[11] R. Colorado Jr., T.R. Lee, J. Phys. Org. Chem. 13 (2000) 796.
[12] A.R. Sandy, S.G.J. Mochrie, D.M. Zehner, K.G. Huang, D. Gibbs, Phys. Rev. B 43 (1991) 4667.
[13] P. Schwartz, F. Schreiber, P. Eisenberger, G. Scoles, Surf. Sci. 423 (1999) 208.
[14] S.M. Wetterer, D.J. Lavrich, T. Cummings, S.L. Bernasek, G. Scoles, J. Phys. Chem. B 102 (1998) 9266.
[15] M. Graupe, T. Koini, V.Y. Wang, G.M. Nassif, R. Colorado Jr., R.J. Villazana, H. Dong, Y.F. Miura, O.E. Shmakova, T.R. Lee, J. Fluorine Chem. 93 (1999) 107.
[16] R.G. Nuzzo, L.H. Dubois, D. Allara, J. Am. Chem. Soc. 112 (1990) 558.
[17] R.G. Nuzzo, E.M. Korenic, L.H. Dubois, J. Chem. Phys. 93 (1990) 767.
[18] G.E. Poirier, Langmuir 13 (1997) 2019.
[19] M.H. Dishner, J.C. Hemminger, F.J. Feher, Langmuir 13 (1997) 2318.
[20] M.H. Dishner, Langmuir 14 (1998) 6676.
[21] K. Erdinger, A. Gölzhäuser, K. Demota, Ch. Wöll, M. Grunze, Langmuir 9 (1993) 4.
[22] D. Seebach, Angew. Chem. Int. Ed. Engl. 29 (1990) 1320.
[23] M. Tolan, X-Ray Scattering from Soft-Matter Thin Films, Springer, Berlin, 1999.
[24] P. Fenter, A. Eberhardt, K.S. Liang, P. Eisenberger, J. Chem. Phys. 106 (1997) 1600.
[25] G.E. Poirier, Langmuir 15 (1999) 1167.
[26] N. Camillione III, T.Y.B. Leung, P. Schwartz, P. Eisenberger, G. Scoles, Langmuir 12 (1996) 2737.
[27] C. Schönenberger, J. Jorritsma, J.A.M. Sondag-Huethorst, L.G.J. Fokkink, J. Phys. Chem. 99 (1995) 3259.
[28] E. Delamarche, B. Michel, Ch. Gerber, D. Anselmetti, H.-J. Güntherodt, H. Wolf, H. Ringsdorf, Langmuir 10 (1994) 2869.
[29] A. Selloni, P. Carnevali, E. Tosatti, C.D. Chen, Phys. Rev. B 31 (1985) 2602.
[30] M.P. Everson, L.C. Davis, R.C. Jaklevic, W. Shen, J. Vac. Sci. Technol. B 9 (2) (1991) 891.
[31] L. Houssiau, M. Graupe, R. Colorado Jr., H.I. Kim, T.R. Lee, S.S. Perry, J.W. Rabalais, J. Chem. Phys. 109 (1998) 9134.